

Gravitational Lens Time Delays in CDM

C.S. Kochanek

Harvard-Smithsonian Center for Astrophysics, 60 Garden Street, Cambridge, MA 02138

email: ckochanek@cfa.harvard.edu

ABSTRACT

In standard CDM halo models, the time delay of a gravitational lens is determined by the cold baryon mass fraction, $f_b = \Omega_{b,cold}/\Omega_0$, of the visible galaxy relative to the overall halo. The observed time delays in PG1115+080, SBS1520+530, B1600+434 and HE2149–2745 give Hubble constants consistent with the HST Key Project value of $H_0 = 72 \pm 8$ km/s Mpc only if $f_b \gtrsim 0.2$ (1-sided 68% confidence), which is larger than the upper bound of $f_{b,max} = \Omega_b/\Omega_0 = 0.15 \pm 0.05$ estimated from the CMB. If all available baryons cool and $f_b = f_{b,max}$ then the time delays imply $H_0 = 65 \pm 6$ km/s Mpc (95% confidence). If local inventories of cold baryons, $f_b \simeq 0.013/h_{70}$, are correct, then $H_0 = 52 \pm 6$ km/s Mpc and the halo parameters closely match isothermal mass models. Isothermal models are also consistent with strong and weak lens studies, stellar dynamics and X-ray observations on these scales, while significantly more centrally concentrated models are not. There is a conflict between gravitational lens time delays, the local distance scale and standard CDM halo models.

Subject headings: cosmology: gravitational lensing; cosmology: Hubble constant; dark matter

1. Introduction

Kochanek (2002a) found that it was difficult to reconcile the time delays measured for 5 simple, well-observed gravitational lenses with the local distance scale given our expectation that galaxies have massive, extended dark matter halos. If the lens galaxies had constant mass-to-light (M/L) ratios we found $H_0 = 71 \pm 6$ km/s Mpc, which is consistent with the local estimate of $H_0 = 72 \pm 8$ km/s Mpc by the HST Key Project (Freedman et al. 2001). However, if the lenses had isothermal mass distributions (flat rotation curves), we found $H_0 = 48_{-4}^{+7}$ km/s Mpc, which is grossly inconsistent with the HST Key Project. While the time delay lenses cannot distinguish between these two limiting mass distributions, models of other lenses (e.g. Munoz, Kochanek & Keeton 2001), stellar dynamical measurements (e.g. Rix et al. 1997, Romanowsky & Kochanek 1999, Gerhard et al. 2001, Treu & Koopmans 2002), weak lensing (e.g. Guzik & Seljak 2002) and X-ray (e.g. Fabbiano 1989, Lowenstein & White 1999) measurements all suggest

that the isothermal mass distributions are correct. In this study we will show that standard cold dark matter (CDM) halo models closely resemble the isothermal models on these scales, which implies there is a conflict between the local distance scale, gravitational lens time delays and CDM halo models.

While the Kochanek (2002a) results provided evidence for a real conflict given the considerable observational evidence that lens galaxies must have extended, massive dark matter halos, the link to a problem with CDM halo models was qualitative because the study lacked a quantitative, theoretical prediction for the time delays expected from CDM halos. One barrier to making such predictions was that we lacked a clear understanding of which features of lens mass distributions control time delays. While global degeneracies due to the addition of constant mass density sheets (e.g. Falco, Gorenstein & Shapiro 1985, Gorenstein, Falco & Shapiro 1988, Saha 2000) and a correlation between more compact mass distributions and longer time delays (e.g. Schechter 2000, Witt, Mao & Keeton 2000) were well known, it was unclear which properties of a halo model had to be accurately computed in order to make robust predictions. Kochanek (2002b) combined analytic results with comparisons to the numerical models by Kochanek (2002a) to show that the surface density in the annulus between the images used to measure the delay was the most important physical property of the lens galaxy for determining the time delay. The interior mass is implicit in the astrometry of the images and the lens galaxy, and the angular structure is either unimportant or strongly constrained by the astrometry. As a result, the Hubble constant expected for a simple lens is related to the surface density by $H_0 = A(1 - \langle\kappa\rangle) + B(\eta - 1)\langle\kappa\rangle$, where $\langle\kappa\rangle$ is the average surface density in the annulus between the images (in units of the critical density), with a modest correction $|B| \lesssim A/10$ due to the logarithmic slope η of the surface density distribution within the annulus ($\kappa \propto R^{1-\eta}$). The coefficients A and B depend only on the image positions and the measured time delay. These simple semi-analytic scaling laws reproduce full numerical models to accuracies of better than 5%.

We can now calculate the expected properties of gravitational lens time delays for CDM halo models. In §2 we outline our model for the halos, which are based on the CDM lens models from Keeton (2001). The models consist of a Hernquist (1990) model for the luminous early-type lens galaxy embedded in an NFW (Navarro, Frenk & White 1996) halo normalized using the parameter estimates of Bullock et al. (2001). We considered both unmodified NFW halos and adiabatically compressed (Blumenthal et al. 1986) halos. We summarize the mathematical details of the model in §2. In §3 we apply it to the four simple time delay lenses PG1115+080, SBS1520+530, B1600+434 and HE2149–2745, to show that the values of $\langle\kappa\rangle$ and η that determine the Hubble constant given the measured time delays are in turn determined by a single parameter, the cold baryonic mass fraction, $f_b = \Omega_{b,cold}/\Omega_0$, of the luminous galaxy compared to the halo. Since the baryon fraction is bounded by local estimates from observed baryonic populations and the global baryon fraction estimated either in clusters or from the CMB, we can set firm bounds for the range of H_0 consistent with CDM halo models. As we discuss in §4, this leads to a new element of the so-called “dark matter crisis” (e.g. Moore 2001), because the CDM halo models combined

with the measured time delays require lower Hubble constants than are consistent with the Key Project estimates based on the local distance scale. An Appendix briefly discusses the effects of tidal truncation on lens galaxy halos.

2. The CDM Lensing Model

Our model for lensing by galaxies with standard CDM halos follows that of Keeton (2001). These models are very similar to the lens models used by Kochanek & White (2001) or those used in semi-analytic models for the structure of galaxies (e.g. Mo, Mao & White 1998, Cole et al. 2000, Gonzalez et al. 2000 and references therein), but focus on early-type rather than late-type galaxies. We model the visible lens galaxy with a Hernquist (1990) profile,

$$\rho_H(r) = \frac{M_H}{2\pi} \frac{r_H}{r(r+r_H)^3}, \quad (1)$$

with the scale length of $r_H = 0.551R_e$ that matches the Hernquist profile to a de Vaucouleurs profile with effective radius R_e . The enclosed mass of the Hernquist model is

$$M_H(< r) = M_H \frac{r^2}{(r+r_H)^2}. \quad (2)$$

We model the initial dark matter halo using an NFW (Navarro, Frenk & White 1996) profile,

$$\rho_N(r) = \frac{M_{vir}}{4\pi f(c)} \frac{1}{r(r+r_s)^2}, \quad (3)$$

normalized by the mass M_{vir} inside the radius r_{vir} with concentration $c = r_{vir}/r_s$ and $f(c) = \ln(1+c) - c/(1+c)$. The enclosed mass is

$$M_N(< r) = M_{vir} f(r/r_s)/f(c). \quad (4)$$

We need the properties of these potentials in projection for the lensing calculations. If we define $\mathcal{F}(x) = |x^2 - 1|^{-1/2} \text{tann}^{-1} |x^2 - 1|^{1/2}$, where the $\text{tann}^{-1} \rightarrow \tan^{-1}$ (\tanh^{-1}) for $x > 1$ ($x < 1$), then the projected surface density of the Hernquist profile is

$$\Sigma_H(x = R/r_H) = \frac{M_H}{2\pi r_H^2} \frac{(2+x^2)\mathcal{F}(x) - 3}{(x^2-1)^2} = \frac{M_H}{r_H^2} \hat{\Sigma}_H(x) \quad (5)$$

and the mass inside cylindrical radius R is

$$M(< x = R/r_H) = M_H \frac{x^2(1-\mathcal{F}(x))}{x^2-1} = M_H \hat{M}_H(< x) \quad (6)$$

(Hernquist 1990, Keeton 2001). Similarly, the projected properties of the NFW model are

$$\Sigma_N(x = R/r_s) = \frac{M_{vir}}{2\pi r_s^2 f(c)} \frac{1-\mathcal{F}(x)}{x^2-1} = \frac{M_{vir}}{r_s^2} \hat{\Sigma}_N(x) \quad (7)$$

and

$$M_N(< x = R/r_s) = \frac{M_{vir}}{f(c)} \left[\ln \frac{x}{2} + \mathcal{F}(x) \right] = M_{vir} \hat{M}_N(< x) \quad (8)$$

for the projected surface density and mass respectively (Bartelmann 1996). The lensing properties of the halo depend on the surface density measured in units of the critical surface density, $\kappa = \Sigma/\Sigma_c$, where the critical surface density, $\Sigma_c = c^2 D_{OS}/4\pi G D_{OL} D_{LS}$, is a simple function of the angular diameter distances between the observer, the lens and the source (e.g. Schneider, Ehlers & Falco 1992).

We need only two observational parameters to normalize the models. The first is the (intermediate axis) effective radius R_e of the lens galaxy, which determines the density distribution of the visible baryons (stars). The second is the critical radius R_c of the lens, determined either by detailed models or simply by the average distance of the images from the lens center, which determines the mass scale. The halo properties depend on the halo concentration, c , virial mass and radius, M_{vir} and r_{vir} , and the mass fraction, f_b , represented by the luminous galaxy. We adopt the halo parameter estimates from Bullock et al. (2001) and an $\Omega_0 = 0.3$ flat cosmological model. The virial mass and radius are related by a definition,

$$M_{vir} = \frac{4\pi}{3} \Delta_{vir}(z) \rho_u(z) r_{vir}^3 = 0.232 \left(\frac{(1+z)r_{vir}}{100h^{-1}\text{kpc}} \right)^3 \left(\frac{\Omega_0 \Delta_{vir}}{200} \right) 10^{12} h M_\odot \quad (9)$$

where $\rho_u(z) = 3H_0^2 \Omega_0 (1+z)^3 / 8\pi G$ is the mean matter density at the lens redshift and the virial overdensity is $\Delta_{vir} \simeq (18\pi^2 + 82x - 39x^2)/\Omega(z)$ where $x = \Omega(z) - 1$. Simulations find that the break radius and the virial radius are statistically correlated through the concentration parameter $c = r_{vir}/r_s$. The average concentration depends on the halo mass M_{vir} and the redshift z ,

$$c = \frac{9}{1+z} \left(\frac{M_{vir}}{8.12 \times 10^{12} h M_\odot} \right)^{-0.14}, \quad (10)$$

but individual halos have a log-normal dispersion about the average concentration of approximately $\sigma_c = 0.18$ (base 10). Finally, a fraction f_b of the mass cools to form the visible galaxy, so the mass of the Hernquist profile is $f_b M_{vir}$ and the remaining mass of the halo is $(1 - f_b) M_{vir}$.

We use the geometry of the lens to determine the overall mass of the halo. The total projected mass inside the critical radius of a spherical lens is $M(< R_c) = \pi R_c^2 \Sigma_c$ (e.g. Schneider et al. 1992), or

$$\pi R_c^2 \Sigma_c = M_{vir} \left[f_b \hat{M}_H(R_c/r_H) + (1 - f_b) \hat{M}_N(R_c/r_s) \right] \quad (11)$$

for a model without adiabatic compression. We combine this equation with the relation between the virial mass and radius (Eqn. 9) to determine M_{vir} and r_{vir} given the cold baryon fraction f_b and the concentration c . The surface density, in units of the critical density, is then

$$\kappa(R) = \frac{M_{vir}}{\Sigma_c} \left[\frac{f_b}{r_H^2} \hat{\Sigma}_H(R/r_H) + \frac{1 - f_b}{r_s^2} \hat{\Sigma}_N(R/r_s) \right], \quad (12)$$

from which we can estimate both the average surface density $\langle\kappa\rangle$ and the logarithmic slope of the surface density η (assuming $\kappa \propto R^{1-\eta}$ locally) in the annulus between the lensed images.

These models probably underestimate the central density of the dark matter because they neglect the compression of the dark matter by the cooling of the baryons. We use the adiabatic compression model (Blumenthal et al. 1986) to compute the changes in the dark matter distribution. For a spherical system with particles on circular orbits, slow changes in the radial mass distribution preserve the angular momentum of the particles. For initial and final radii of r_i and r_f and mass distributions $M_i(< r)$ and $M_f(< r)$, the angular momentum of a circular orbit is conserved if $r_i M_i(< r_i) = r_f M_f(< r_f)$. The initial mass distribution is simply that of the NFW halo, $M_i(< r) = M_N(< r)$. The final mass distribution is

$$M_f(< r_f) = f_b M_H(< r_f) + (1 - f_b) M_A(< r_f) = f_b M_H(< r_f) + (1 - f_b) M_N(< r_i) \quad (13)$$

where the final halo mass distribution $M_A(< r_f) = M_{vir} \hat{M}_A(< r_f)$ is the same as that of the original halo at the initial radius $M_N(< r_i)$. For the compression of a NFW halo by Hernquist galaxy, the solution for $r_f(r_i)$ is analytic (a cubic equation, see Keeton 2001). Jesseit et al. (2002) show that simple Blumenthal et al. (1986) model accurately estimates the changes in the mass distribution. The compressed halo density profile must then be numerically projected to determine the projected mass

$$M_A(< R) = M_{vir} \hat{M}_A(< R) = M_{vir} \int_0^{\pi/2} d\phi \cos \phi \hat{M}_A(< r = R \sec \phi) \quad (14)$$

and surface density

$$\Sigma_A(R) = \frac{M_{vir}}{r_s^2} \hat{\Sigma}_A(R) = \frac{M_{vir}}{2\pi R} \int_0^{\pi/2} d\phi \frac{d\hat{M}_A}{dr}(< r = R \sec \phi), \quad (15)$$

and then we must solve Eqns. (11) and (12) for M_{vir} and r_{vir} with the NFW profile replaced by the adiabatically compressed profile. For one lens, B1600+434, we include an exponential disk as well as a bulge in the baryonic model, fixing the mass ratio to that inferred from the constant M/L mass models of Kochanek (2002a). Once we have determined the surface density, we can easily calculate the mean surface density $\langle\kappa\rangle$ and the logarithmic slope η of the surface density in the annulus between the images for which time delays have been measured.

In addition to estimates of the Hubble constant, we can also calculate the weak lensing aperture mass, $\Delta\Sigma(R) = \langle\Sigma(< R)\rangle - \Sigma(R)$, from the surface density profile. Because weak lensing measurements are made on much larger scales ($R \gtrsim 50h^{-1}$ kpc) than the critical radius of the lens ($R \simeq 5h^{-1}$ kpc), they provide a nearly ideal additional constraint on the extent and mass of the dark matter halo. Compact, low-mass, constant M/L models will produce smaller weak lensing signals than extended, high-mass, dark matter dominated models. While there are no weak lensing measurements for time delay lenses, we can estimate the expected signal from the measurements by the Sloan Digital Sky Survey (SDSS, McKay et al. 2001, Guzik & Seljak 2002).

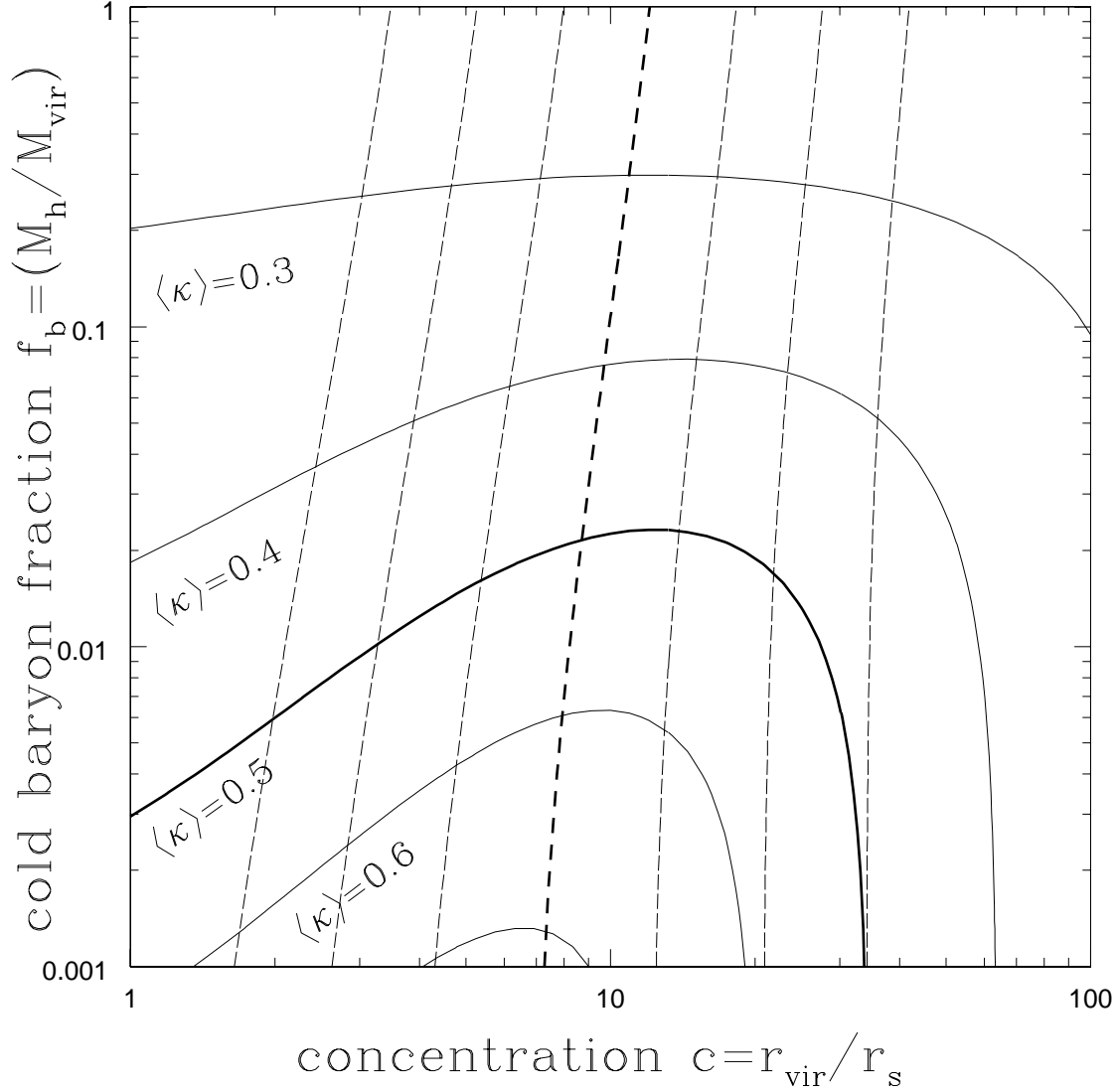


Fig. 1.— The average surface density $\langle \kappa \rangle$ for adiabatically compressed models of HE2149–2745 as a function of the halo concentration $c = r_{vir}/r_s$ and the mass fraction in the cold baryons of the visible galaxy $f_b = M_H/M_{vir}$. The solid lines are contours of $\langle \kappa \rangle$ spaced at intervals of $\Delta\langle \kappa \rangle = 0.1$. An isothermal model has $\langle \kappa \rangle = 0.5$ (the heavy solid contour). Constant M/L models lie on the top edge where $f_b = 1$. In the Bullock et al. (2001) simulations of halo formation, halos have a limited range of concentrations for a given virial mass. The heavy dashed contour shows the most likely halo concentration, and the light dashed contours show the 1, 2 and 3σ ranges for the concentration distribution.

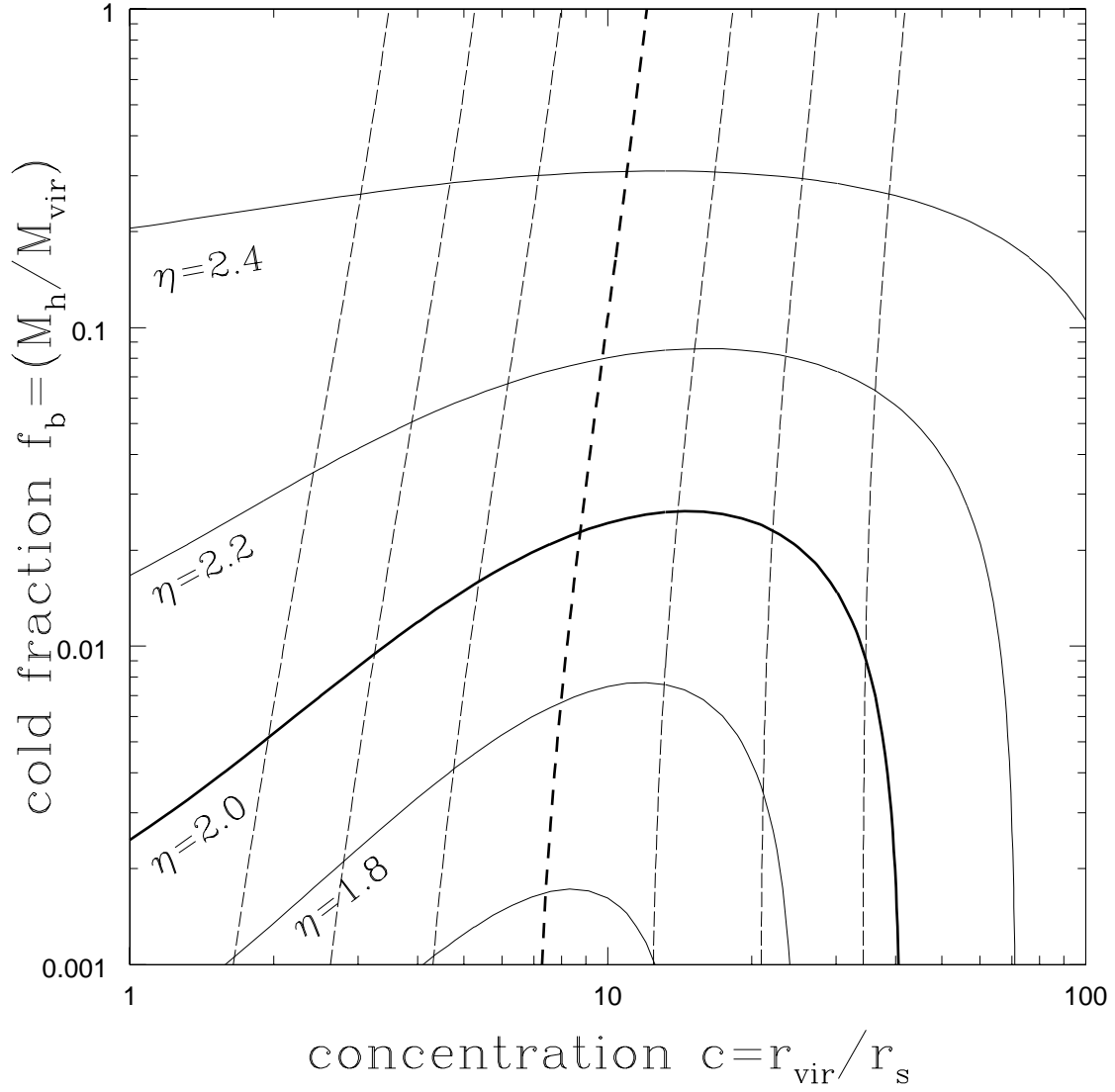


Fig. 2.— The average logarithmic slope η in the annulus between the images ($\kappa \propto R^{1-\eta}$) for adiabatically compressed models of HE2149–2745 as a function of the halo concentration $c = r_{vir}/r_s$ and the mass fraction in cold baryons of the visible galaxy $f_b = M_H/M_{vir}$. The solid lines are contours of η spaced at intervals of $\Delta\eta = 0.2$. An isothermal model has $\eta = 2$ (the heavy solid contour). The dashed contours show the likelihood of the concentration. The heavy dashed contour is the average concentration given the virial mass and the light dashed contours show the 1, 2 and 3σ ranges for the concentration (see Fig. 1).

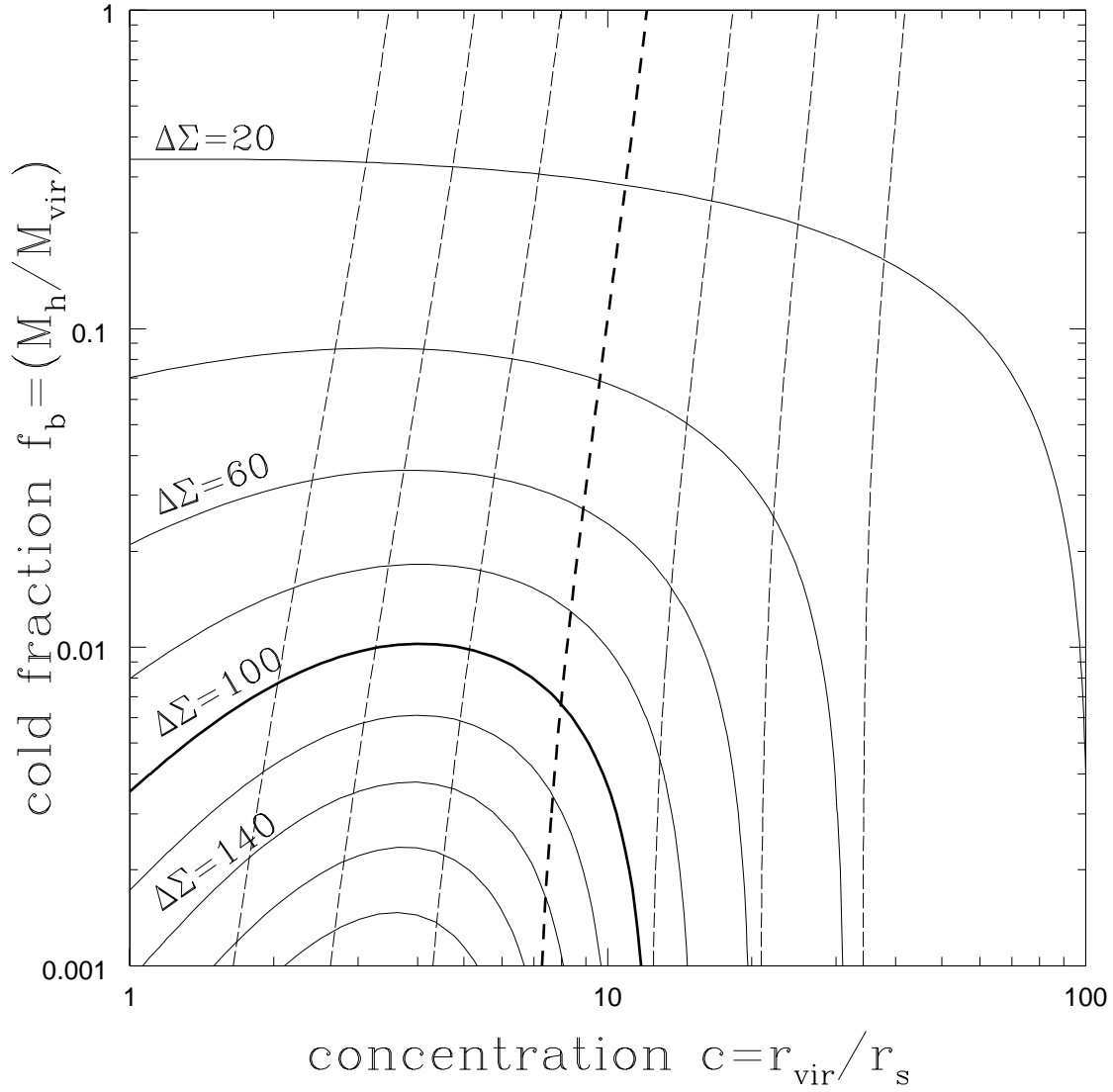


Fig. 3.— The weak lensing surface density $\Delta\Sigma$ at $R_w = 75h^{-1}$ kpc for HE2149–2745 as a function of the halo concentration $c = r_{vir}/r_s$ and the mass fraction in cold baryons of the visible galaxy $f_b = M_H/M_{vir}$. The solid lines are contours of $\Delta\Sigma$ spaced at intervals of $20hM_\odot/\text{pc}^2$ with a heavy contour for the surface density expected from the SDSS weak lensing results, $\Delta\Sigma_{SDSS} \simeq 100hM_\odot/\text{pc}^2$. An isothermal model would have $\Delta\Sigma_{SDSS} \simeq 70hM_\odot/\text{pc}^2$. Based on the virial mass of each model, the dashed contours show the likelihood of the concentration. The heavy dashed contour is the average concentration given the virial mass and the light dashed contours show the 1, 2 and 3σ ranges for the concentration (see Fig. 1).

We consider only the innermost $R_w = 75h^{-1}$ kpc bin of the SDSS measurements in order to minimize contamination of the signal from sources other than the galaxy halo. In addition to any intrinsic uncertainties in the SDSS results, the conversion of the results into a constraint on our models is complicated. We assume that we can estimate the central stellar velocity dispersion of the lens galaxy using an SIS lens model, which appears to be a fairly reliable assumption (see Kochanek et al. 2000, Treu & Koopmans 2002). We then use the observed properties of early-type galaxies in the SDSS (Bernardi et al. 2002) to convert the velocity dispersion into estimates for the r' and i' magnitudes the lens galaxy would have locally. This avoids any problems of luminosity evolution at the price of introducing the roughly 1 mag of scatter in the Faber-Jackson relation. Combining these magnitudes with the r' and i' magnitude zero points from Blanton et al. (2001) and a fit to the $\Delta\Sigma(R)$ measurements in McKay et al. (2001), we estimate that the SDSS weak lensing results correspond to a constraint on the aperture mass of

$$\Delta\Sigma_{SDSS}(R_w = 75h^{-1}\text{kpc}) \simeq 80 \left(\frac{\sigma}{200\text{km/s}} \right)^{3.2} hM_{\odot}/\text{pc}^2 \quad (16)$$

with a crudely estimated uncertainty of a factor of two. That the weak lensing signal is dominated by the galaxies has been checked by showing that the dynamics of satellites around the target galaxies confirm the mass estimates (McKay et al. 2002). Future analyses of weak lensing in the SDSS, particularly segregating the galaxies by velocity dispersion rather than luminosity, will clarify the scalings and the uncertainties. As a reality check of this scaling, a singular isothermal sphere of velocity dispersion σ predicts $\Delta\Sigma = 62(\sigma/200\text{km/s})^2 hM_{\odot}/\text{pc}^2$, and suggests that the scaling of the SDSS results is somewhat high. For now, the weak lensing results provide an interesting, but not a definitive, constraint on the halo properties.

3. Results

We use the four simple, well-characterized time delay lenses PG1115+080 (Schechter et al. 1997, Barkana 1997, Impey et al. 1998), SBS1520+530 (Burud 2002b, Faure et al. 2002), B1600+434 (Burud et al. 2000, Koopmans et al. 2000) and HE2149–2745 (Burud et al. 2002) for our analysis, using the Hubble constant scalings derived in Kochanek (2002b). Of the remaining 5 time delay lenses, B0218+357 lacks an accurate measurement of the position of the lens galaxy (Lehar et al. 2000), B1608+656 has two interacting lens galaxies (Koopmans & Fassnacht 1999), Q0957+561 and RXJ0911+0551 are too heavily perturbed by their parent clusters for our simple scaling with the surface density (see Kochanek 2002b), and the properties of the lens galaxy in PKS1830–211 are in dispute (Winn et al. 2002, Courbin et al. 2002). For each lens we model the baryonic distribution using the photometric profiles scaled by their intermediate axis scale lengths (the geometric mean of the major and minor axes). Since the masses are determined by the lens geometry, this is the only observational property of the lens galaxy needed for our calculation. The results are insensitive even to large (50%) changes in the scale length. The only important uncertainties in the measurements are the time delays and the B1600+434 lens galaxy position.

Figures 1 and 2 show the expected values for $\langle\kappa\rangle$ and η in HE2149–2745 as a function of the cold baryon fraction f_b and the halo concentration $c = r_{vir}/r_s$. For each value of f_b and c , the virial mass (and radius) are determined by the observed critical radius of the lens. As the cold baryon fraction $f_b \rightarrow 1$, the surface density converges to that of a constant M/L model and the density exponent is relatively steep ($\eta \simeq 2.5$). The images lie somewhat outside the effective radius of the lens ($R_e = 0''.48$, $R_c = 0''.85$, $R_1 = 0''.34$ and $R_2 = 1''.35$) so the average slope of the surface density is closer to the outer density exponent ($\eta = 4$) than the inner density exponent ($\eta = 1$) of the Hernquist profile (Eqn. 1). As we lower the cold baryon fraction f_b , the expected surface density $\langle\kappa\rangle$ rises and the slope η flattens. They reach the isothermal values, $\langle\kappa\rangle = 1/2$ and $\eta = 2$, for baryon fractions $f_b \simeq 0.025$. Very extended halos (small c) are too diffuse, and very compact halos (large c) are too compact to contribute to $\langle\kappa\rangle$.

In simulations, halos with a fixed virial mass are found to have a limited range of concentrations (see Bullock et al. 2001 and Eqn. 10), so only a portion of the f_b – c plane can be occupied by real halos. We find that the theoretically expected range of concentrations for the lenses ($c \simeq 10$) depends little on the cold baryon fraction, as we can see in Figs. 1 and 2 from the superposed contours for the expected range of concentrations given by the Bullock et al. (2001) results. As a result, the lensing properties depend almost exclusively on the cold baryon fraction. If we do not include the adiabatic compression of the halo the results change slightly, but the results are similar because the estimates with and without compression must be the same in the limits of both large and small baryon fractions.

Figure 3 shows the expected strength of the weak lensing signal $\Delta\Sigma$ measured $R_w = 75h^{-1}$ kpc from the lens. The aperture mass/surface density which determines the measured weak lensing shear steadily declines as we increase the cold baryon fraction and the total halo mass decreases. This means that the amplitudes of the shears measured by weak lensing provide a convenient observational constraint on the cold baryon fraction. Implementing this in practice is difficult, but for the scalings leading to Eqn. (16) we predict that $\Delta\Sigma_{SDSS} \simeq 100hM_\odot/\text{pc}^2$ for HE2149–2745 given the 214 km/s velocity dispersion estimated from the image separations. With our rough estimate of (logarithmic) uncertainties of a factor of two, the discriminatory power of the weak lensing estimates is limited but favors models with substantial amounts of dark matter. Like the values for $\langle\kappa\rangle$ and η , we can largely describe the weak lensing amplitude simply by the cold baryon fraction.

The restricted range of permitted concentrations and the weak dependence of the lens properties on the concentration in that range allows us to simplify the results by considering only the concentration probability averaged values for $\langle\kappa\rangle$ and η as a function of f_b . Figs. 4 and 5 show the expected values of $\langle\kappa\rangle$ and η as a function of the cold baryon fraction for PG1115+080, SBS1520+530 B1600+434 and HE2149–2745. For a fixed cold baryon fraction f_b , the results for the four lenses are similar, the differences between adiabatically compressed and uncompressed models are small and the scatter due to the permitted range of concentrations is still smaller. Over the range of baryon fractions from $f_b = 10^{-3}$ to $f_b = 1$, the expected surface density decreases

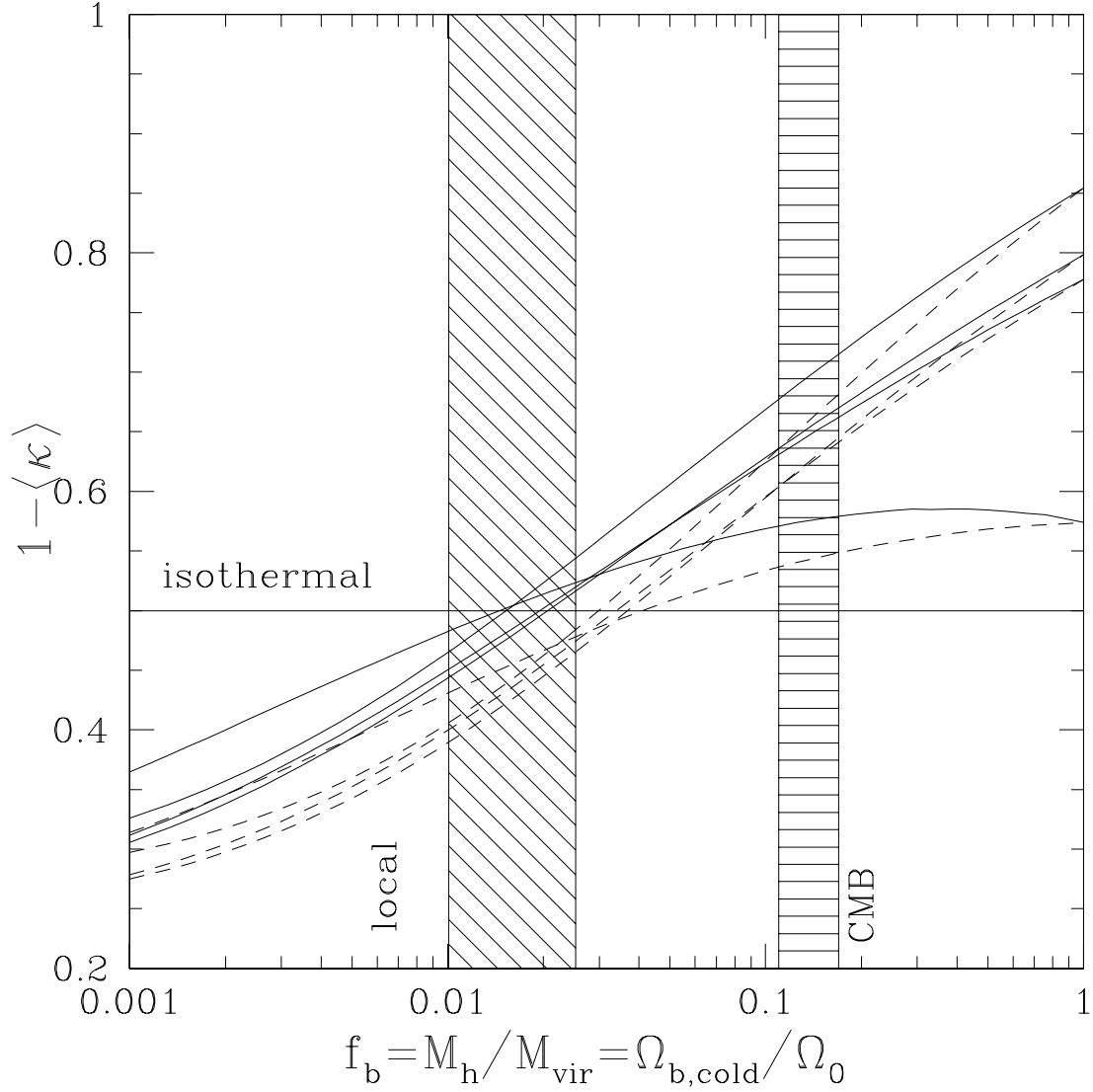


Fig. 4.— The concentration-averaged estimates for $1 - \langle \kappa \rangle$ as a function of f_b for PG1115+080, SBS1520+530, B1600+434 and HE2149–27145. The solid (dashed) curves are for models with (without) adiabatic compression. A horizontal line shows the value expected for isothermal models. The diagonally cross-hatched region shows the lower bound on f_b based on the local inventory of cold baryons by Fukugita et al. (1998) for $H_0 = 60$ km/s Mpc and $\Omega_0 = 0.3$. The horizontally cross-hatched region shows the upper bound on f_b set by the global ratio of Ω_b/Ω_0 estimated from the CMB.

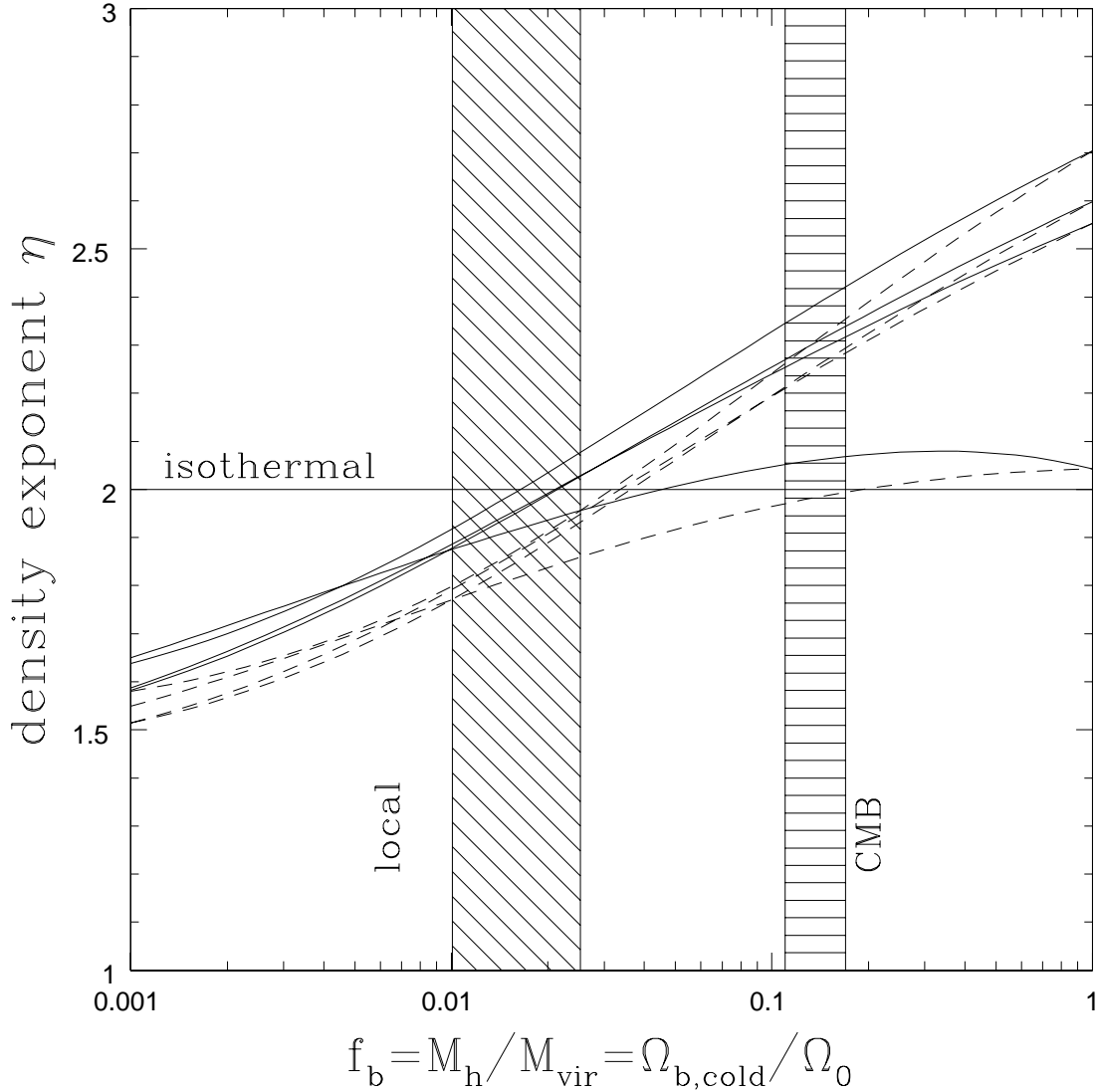


Fig. 5.— The concentration-averaged estimates for the annular density exponent η ($\kappa \propto R^{1-\eta}$) as a function of f_b for PG1115+080, SBS1520+530, B1600+434 and HE2149–27145. The solid (dashed) curves are for models with (without) adiabatic compression. A horizontal line shows the value expected for isothermal models. The limits on f_b are the same as in Fig. 4.

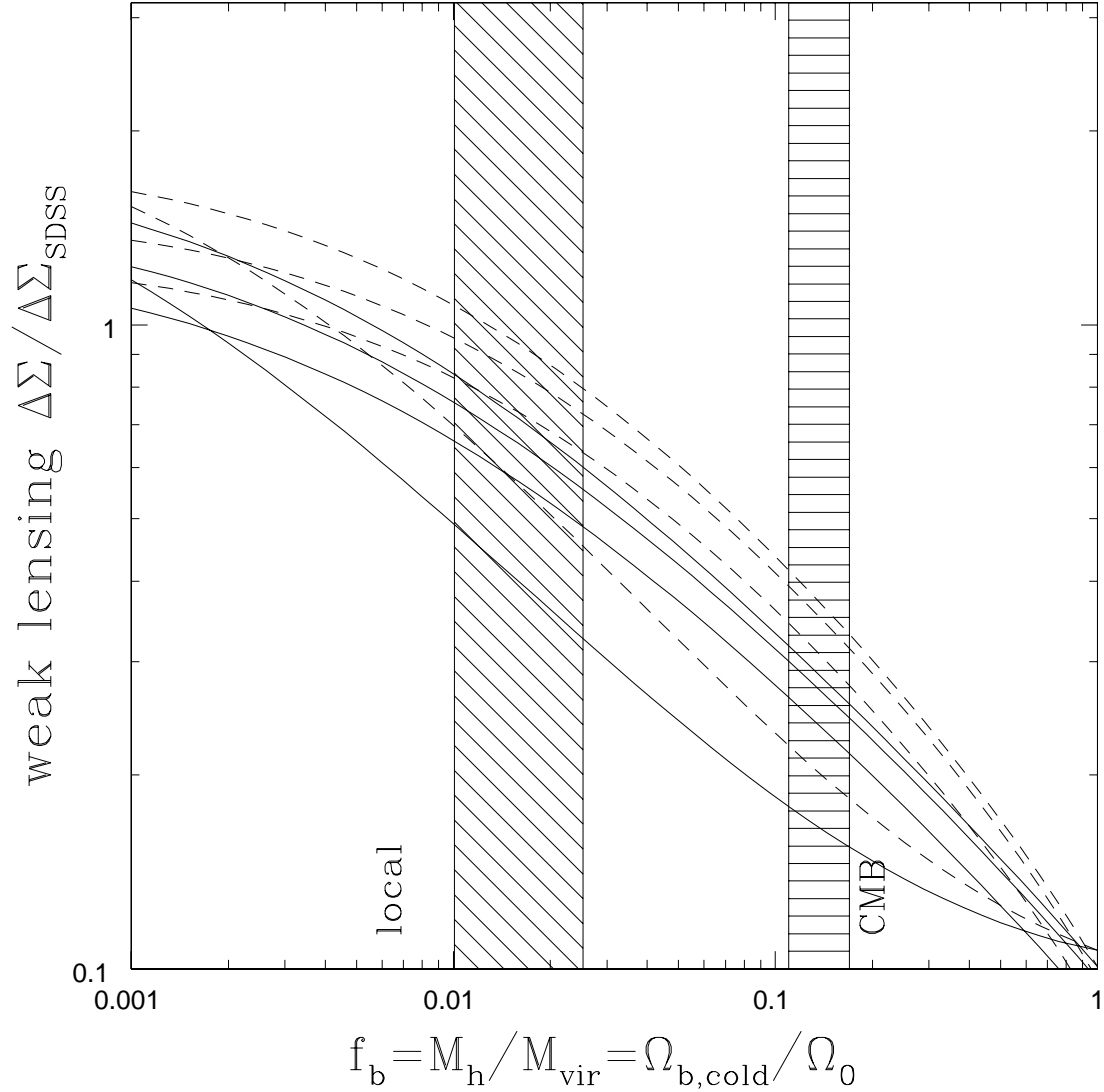


Fig. 6.— The concentration-averaged estimates for the ratio $\Delta\Sigma/\Delta\Sigma_{SDSS}$ between the expected weak lensing signal $\Delta\Sigma$ and our best estimate of the SDSS measurements $\Delta\Sigma_{SDSS}$ for galaxies with the velocity dispersion of the lens. The normalization of $\Delta\Sigma_{SDSS}$ is uncertain to a factor of 2 (0.3 dex). The solid (dashed) curves are for models with (without) adiabatic compression. The limits on f_b are the same as in Fig. 4.

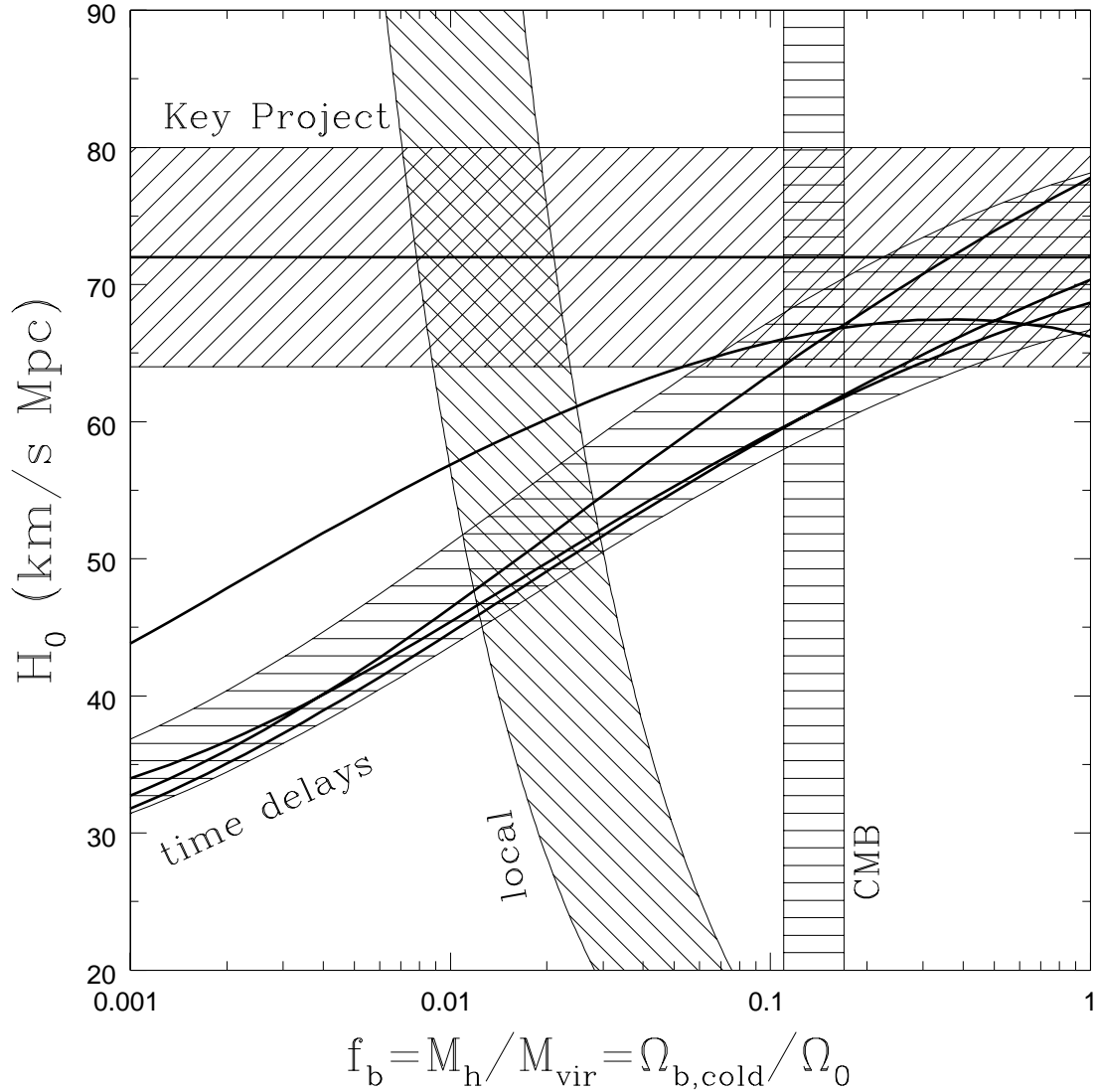


Fig. 7.— The Hubble constant as a function of f_b for the lenses PG1115+080, SBS1520+530, B1600+434 and HE2149–27145. The heavy curves show the results for the individual lenses including adiabatic compression. The shaded envelope bracketing the curves is the 95% confidence region for the combined lens sample. The vertical bands show the lower bound on f_b from local inventories, including its H_0^{-1} scaling, and the upper bound from the CMB. The horizontal band shows the estimate of $H_0 = 72 \pm 8$ km/s Mpc by the HST Key Project (Freedman et al. 2001). Without adiabatic compression, the estimates from the time delays predict values for H_0 approximately 5 km/s Mpc lower.

from $\langle \kappa \rangle \simeq 0.7$ to $\langle \kappa \rangle \simeq 0.2$ and the exponent of the density profile steepens from $\eta \simeq 1.6$ to $\eta \simeq 2.6$. B1600+434 behaves differently because it has a smaller ratio between the Einstein radius and the half-light radius than the other three systems.

The cold baryon fraction, $f_b = M_H/M_{vir} = \Omega_{b,cold}/\Omega_M$, is set by the cosmological density $\Omega_{b,cold}$ of baryons that have cooled enough to be modeled by the visible galaxy compared to the total density of baryons and dark matter Ω_M . Local accountings for cold baryons (stars, remnants, cold gas components) by Fukugita, Hogan & Peebles (1998) estimated that $0.0024/h_{70} \lesssim \Omega_{b,cold} \lesssim 0.0064/h_{70}$, which sets a Hubble constant-dependent lower bound that $f_b \gtrsim 0.01$ for $\Omega_0 = 0.3$. The global ratio of Ω_b/Ω_0 sets an upper bound on the cold baryon fraction. If clusters of galaxies contain a fair sample of material (White et al. 1993), their baryonic mass fraction determines $\Omega_b/\Omega_0 \simeq (0.113 \pm 0.005)(1 + 0.22h_{70}^{1/2})h_{70}^{-3/2}$ where the numerical estimate is from the recent study of Allen, Schmidt & Fabian (2002). Current analyses of the cosmic microwave background (CMB) anisotropies find $\Omega_b/\Omega_0 \simeq 0.15 \pm 0.05$ (e.g. Netterfield et al. 2002, Wang, Tegmark & Zaldarriaga 2002), consistent with the cluster inventory results. In this context we should also note that the CMB analyses generally favor lower Hubble constants than the Key Project estimates. The local baryon inventory and the global ratio Ω_b/Ω_0 set upper and lower bounds on the cold baryon fraction f_b appropriate for our models. The cold baryon fraction could be substantially higher than observed locally at the price of introducing a cold but locally unobserved baryonic population. We have superposed these local and global limits on f_b on Figs. 4 and 5.

For baryon fractions similar to local inventories ($f_b \sim 0.02$), the surface density $\langle \kappa \rangle$ and logarithmic slope η are remarkably close to the isothermal values of $\langle \kappa \rangle = 1/2$ and $\eta = 2$. For PG1115+080, SBS1520+530, B1600+434 and HE2149–2745 we find $\langle \kappa \rangle = 0.50 \pm 0.05$, 0.52 ± 0.04 , 0.50 ± 0.03 , and 0.52 ± 0.04 respectively, and $\eta = 1.98 \pm 0.09$, 1.95 ± 0.09 , 1.91 ± 0.05 , and 1.95 ± 0.09 respectively if we constrain f_b by the local values scaled to $H_0 = 60$ km/s Mpc. This means that our standard isothermal lens model, which represent our best independent estimate of the mass distribution on these scales, is also the expectation from standard CDM halo models. If we allow larger cold baryonic mass fractions, then the surface densities decrease and the slopes steepen. We find $\langle \kappa \rangle = 0.30 \pm 0.04$, 0.34 ± 0.03 , 0.45 ± 0.11 and 0.35 ± 0.03 , and $\eta = 2.40 \pm 0.06$, 2.32 ± 0.07 , 2.02 ± 0.27 and 2.30 ± 0.05 for PG1115+080, SBS1520+530, B1600+434 and HE2149–2745 respectively when we force $f_b = \Omega_b/\Omega_0 = 0.15 \pm 0.05$. These parameter values lie roughly midway between isothermal and constant M/L mass models.

The expected weak lensing signals, shown in Fig. 6 as the ratio $\Delta\Sigma/\Delta\Sigma_{SDSS}$ between our estimate from the models and our estimate for the SDSS measurements on a scale of $R_w = 75h^{-1}$ kpc, provides one independent test of the models. The weak lensing signal diminishes as f_b increases and the total mass of the halo diminishes. Models with f_b similar to local inventories predict weak lensing signals roughly consistent with the SDSS measurements (about 70% of the expected amplitude, but we only believe the scaling to a factor of two at present). If all available baryons cool, the expected weak lensing signal is too weak to agree with the SDSS measurements

(only 30% of the expected amplitude). Models with constant M/L predict weak lensing signals only 10% of the expected amplitude and are strongly ruled out. With a factor of two uncertainty, the weak lensing constraint formally restricts the models to the range $0.002 \lesssim f_b \lesssim 0.015$ (90% confidence). Note that when Keeton (2001) used these lens models to fit the distribution of image separations in lens surveys, he found it was difficult to match the observed separation distributions for $f_b \lesssim 0.1$.

Finally, in Fig. 7 we use the estimates of $\langle \kappa \rangle$ and η for the CDM halo models to estimate the Hubble constant as a function of f_b for PG1115+080, SBS1520+530, B1600+434 and HE1149–2745.¹ As we would expect from the homogeneity of the lenses (see Kochanek 2002b), these four lenses predict similar values of H_0 as a function of f_b . For low f_b , B1600+434 gives somewhat higher values for H_0 than the other three lenses. The joint estimate has small statistical uncertainties (5%) compared to the overall variable range. If the baryon density is restricted to agree with the local baryon inventory, then $H_0 = 52 \pm 6$ km/s Mpc (formally at 95% confidence), and if it is restricted to agree with the global baryon inventory, then $H_0 = 65 \pm 6$ km/s Mpc. Restricted by the SDSS weak lensing results rather than f_b , we find that $H_0 = 43 \pm 7$ km/s Mpc, but much of the lower range has baryon fractions below that found in local inventories. If we combine the weak lensing constraints with the lower bounds on f_b from the local inventories, we find that $H_0 = 48 \pm 5$ km/s Mpc. The limits for models without adiabatic compression are approximately 5 km/s Mpc lower.

Superposed on Fig. 7 is the local estimate of $H_0 = 72 \pm 8$ km/s Mpc by the HST Key Project (Freedman et al 2001). The local estimate is consistent with these four lenses only in the limit of a constant M/L , as we had found previously (Kochanek 2002a). Formally, agreement with the Key Project requires $f_b > 0.06$ (one-sided, 95% confidence). It is slightly inconsistent with models in which all baryons cool, and grossly inconsistent with models having realistic baryon fractions or weak lensing signals consistent with the SDSS measurements.

4. Discussion

Because gravitational lens time delays are determined by the Hubble constant and the average surface density $\langle \kappa \rangle$ of the lens galaxy in the annulus between the images (Kochanek 2002b), we can make unambiguous estimates for the behavior of time delays in standard CDM halo models. In

¹The scaling solutions from Kochanek (2002b) for these lenses are $H_0 = A(1 - \langle \kappa \rangle) + B\langle \kappa \rangle(\eta - 1)$ where the coefficients (A , B) in units of km s/Mpc for the lenses are (92.3, 4.6), (93.2, 10.5), (103.9, 20.6) and (84.4, 13.6) for PG1115+080, SBS1520+530, B1600+434 and HE1149–2745 respectively, and they produce fractional errors in H_0 due to uncertainties in the astrometry and the time delays of 9%, 6%, 9% and 13%, respectively, after broadening the errors in the time delays to a minimum of 5% to encompass systematic effects such as convergence fluctuations from large scale structure (e.g. Seljak 1994, Barkana 1996). PG1115+080 is in a group which supplies an additional external convergence of $\kappa_{ext} = 0.2(1 - \langle \kappa \rangle)$.

these models, the expected delay is controlled by the mass fraction, $f_b = M_H/M_{vir} = \Omega_{b,cold}/\Omega_0$, in cold baryons making up the observed lens galaxy relative to the overall halo. As the cold baryon fraction rises, so does the Hubble constant.

When the cold baryon fraction is comparable to the local baryonic content of galaxies ($f_b \simeq 0.02$, Fukugita et al. 1998), the model parameters closely match those for isothermal (flat rotation curve) dark matter dominated lens models and the halos produce weak lensing signals compatible with weak lensing measurements in the SDSS (McKay et al. 2001). The mean surface density in the annulus is almost exactly $\langle \kappa \rangle = 1/2$ and the local slope of the surface density is almost exactly $\eta = 2$ ($\kappa \propto R^{1-\eta}$). Isothermal models are not only the best observational estimate for the lensing potential on these scales, they are also the model predicted by CDM assuming standard parameters and baryonic populations. For baryon fractions with a lower limit set by the local inventory and the upper limit set by the weak lensing measurements, we find that $H_0 = 48 \pm 5$ km/s Mpc based on the time delays measured for PG1115+080, SBS1520+530, B1600+434 and HE2149–2745. If all baryons were to cool and $f_b \simeq 0.15 \pm 0.05$, based on constraints from either the CMB (e.g. Netterfield et al. 2002, Wang et al. 2002) or cluster baryon fractions (e.g. White et al. 1993, Allen et al. 2002), then the Hubble constant could be as high as $H_0 = 65 \pm 6$ km/s Mpc. Such models require most of the cold baryons in the lens galaxies to be in a locally invisible population and correspond to mass distributions less consistent with direct estimates. Both of these possibilities are lower than the local estimates of $H_0 = 72 \pm 8$ km/s Mpc from the HST Key Project (Freedman et al. 2001), which agrees with the time delays of these four lenses only for mass distributions with constant M/L ratios. Thus, our detailed models for the expected properties of time delays in standard CDM halos agree with our simple models in Kochanek (2002a), and we are faced with a conflict between CDM halo models, gravitational lens time delays and the local distance scale.

While there is some room for error in the lens results, the mutual agreement of the four simple, well-characterized time delay lenses and the simple relation between time delays, surface densities and the Hubble constant makes it difficult to point to a weakness (Kochanek 2002b). The most important observational steps are to improve the accuracies of the existing delay measurements and to expand the number of systems with delay measurements. If the homogeneity of the results for simple lens systems, as compared to more complicated systems in clusters or with interacting galaxies, continues, the case for the existence of a conflict will become overwhelming. Improved characterizations of the lenses, either to constrain the mass distribution in the time delay lenses directly or to allow us to include the five other time delay lenses, are also important, but depend on obtaining deeper HST imaging of the systems. Other constraints on the mass distributions such as weak lensing or the stellar dynamical measurements of the lens galaxies can also help to break any degeneracies. In particular, estimates of the weak lensing signal as a function of the stellar velocity dispersion rather than luminosity would be excellent constraints on the halo extent in time delay lenses.

The systematic uncertainties in the mass distribution can be minimized by measuring time

delays in lenses where the baryons dominate the mass and there is little difference between a constant M/L model and a model with dark matter. This means measuring the time delay in very low redshift lens galaxies where the ratio of the critical radius to the effective radius, $R_c/R_e \propto D_{OL}$ is small and the mass near the Einstein ring is increasingly dominated by the baryons. For example, models of Q2237+0305 at $z_l = 0.04$ suggest that less than 10% of the mass inside the Einstein ring of the lens can be dark, instead of the roughly 50% for typical models of higher redshift lenses (Trott & Webster 2002). Unfortunately, Q2337+0305 has shown no variability on the very short time scale of its expected delay, making it a poor candidate for measuring time delays. There is a certain irony to proposing that local galaxies, which might be incorporated in local distance scale studies, are the ideal time delay lenses, but it may also lead to a system where the local and the “cosmological” distance scales can be compared directly.

Acknowledgments. CSK thanks D. Rusin, P. Schechter, U. Seljak, J. Winn and S. Wyithe for discussions and comments. CSK is supported by the Smithsonian Institution and NASA ATP grant NAG5-9265.

A. Tidal Truncation

Many lens galaxies, including many of the time delay lenses, are group and cluster members (e.g. Keeton, Christlein & Zabludoff 2000). Particularly when PG1115+080 appeared to be the exception among time delay lenses rather than the rule, tidal truncation of its halo by the surrounding group was frequently invoked as a possible explanation for what appeared to be an anomalously low H_0 estimate for isothermal lens models (e.g. Impey et al. 1998, Koopmans & Fassnacht 1999). The idea is that a tidally truncated halo is more centrally concentrated and has a lower $\langle \kappa \rangle$, so it produces a higher estimate of H_0 for a fixed time delay. However, in order to significantly raise H_0 , the halo must have a tidal truncation radius comparable to the critical radius of the lens and the surface density of the truncating halo must be kept low. While orbital history, phase, projection effects and differences in the density distribution make the physics of tidal truncation considerably more complicated than the simple model we discuss, simple scaling laws for tidal truncation suggest that this standard picture is physically implausible.

The first problem with tidal truncation is that it is extraordinarily difficult to truncate the mass distribution of a lens galaxy on scales comparable to the critical radius. For two SIS lenses, the tidal radius of the less massive lens is $R_t = R_p(b_0/b_p)^{1/2}$ when the projected separation is equal to the true separation in three dimensions. The ratio roughly equals the velocity dispersion ratio of the two halos, $(b_0/b_p)^{1/2} \simeq \sigma_0/\sigma_p$, so for the typical massive lens galaxy in a low mass group or cluster the tidal radius $R_t \gtrsim R_p/2$. Truncating the lens galaxy near the Einstein ring is almost impossible because the inequality $R_t < b_0$ implies a galaxy inside the critical radius of the cluster, $R_p < (b_p b_0)^{1/2} < b_p$, where it cannot produce the image geometries seen for isolated lenses. In fact, weak lensing studies of galaxies in the cores of rich clusters have shown that even in these high density environments the halos of the galaxies seem to be truncated only on scales

$\gtrsim 20h^{-1}$ kpc far larger than the $\lesssim 5h^{-1}$ kpc scales on which tidal begins to alter the time delays significantly (Natarajan et al. 2001).

The second problem is that the reduction in $\langle\kappa\rangle$ from tidally truncating the primary lens must be accompanied by an increase in $\langle\kappa\rangle$ from the convergence κ_{ext} of the halo responsible for the truncation. Existing lens models partly incorporate this effect through the scaling of external shears with surface density. As a concrete example, suppose we have a cruciform lens with images on the symmetry axes. We consider two models: an SIS primary lens perturbed by an SIS cluster, and a point mass primary lens perturbed by an SIS cluster. We model the cluster as an equal external shear and convergence, $\gamma = \kappa = b_p/2R_p$, for a cluster with critical radius b_p at impact parameter R_p . For a source directly behind the lens, the two models can produce identical image positions. The critical radius of the primary lens, b_0 , is the same in both models, but the cluster shear for an isothermal primary is less than that for a point mass primary, with $\gamma_{pnt} = \kappa_{pnt} = 2\kappa_{SIS}(1 - \kappa_{SIS}) = 2\gamma_{SIS}(1 - \gamma_{SIS})$. As the lens galaxy becomes more compact, the external shear and convergence from the cluster increase. The time delay ratio depends only on the strength of the cluster perturbation,

$$\frac{\Delta t_{pnt}}{\Delta t_{SIS}} = \frac{1 - \kappa_{SIS}}{\kappa_{SIS}} \ln \left[\frac{1}{1 - 2\kappa_{SIS}} \right] \rightarrow 2(1 - \kappa_{SIS}) + \dots \quad (\text{A1})$$

for small perturbations. The factor of 2 is the ratio of the $\langle\kappa\rangle$ values for a point mass and an isothermal primary lens, and the correction is due to the higher convergence of the cluster when the primary lens is a point mass. The delay ratio is monotonically declining, reaching unity for $\kappa_{SIS} = \gamma_{SIS} = 0.36$ ($\gamma_{pnt} = 0.45$). Thus, as we raise the cluster convergence, so as to make tidal truncation physically plausible, the reduction in H_0 by the cluster convergence eventually becomes more important than the increases in H_0 from making the primary lens more centrally concentrated.

While the rise in κ_{ext} produced by the natural scaling of lens parameters with the increasing concentration of the lens galaxy mimics the effects of tidal truncation, it does not necessarily lead to self-consistent results because the amplitudes of the shear and convergence, γ_{ext} and κ_{ext} , from the perturbing halo are closely related to the tidal truncation radius. For an isothermal galaxy truncated by an isothermal halo, the surface density of the perturber at the tidal radius is $\kappa_{ext} = b_0/2R_t \rightarrow 1/2$ as the tidal radius approaches the critical radius, $R_t \rightarrow b_0$. Equivalently, there is a close relation between the tidal radius and the external shear from the perturbing halo, with $R_t = (b_0 b_p)^{1/2}/2\gamma_{ext}$ for two isothermal halos, which means that the truncation radius cannot be close to the Einstein ring unless the external shear is large. Hence, the standard parameters of “tidally truncated” models of PG1115+080, where $\kappa_{ext} = \gamma_{ext} \simeq 0.15$ are inconsistent with simple models of the group parameters required to tidally truncate the lens galaxy. The standard model will tend to overestimate H_0 for tidally truncated galaxies by underestimating κ_{ext} .

REFERENCES

- Allen, S.W., Schmidt, R.W., & Fabian, A.C., 2002, MNRAS submitted [astro-ph/0205007]
- Barkana, R., 1996, ApJ, 468, 17
- Barkana, R., 1997, ApJ, 489, 21
- Bartelmann, M., 1996, A&A, 313, 697
- Bernardi, M., et al., 2002, AJ submitted [astro-ph/0110344]
- Blanton, M.R., et al., 2001, ApJ, 121, 2358
- Blumenthal, G., Faber, S., Flores, R., & Primack, J., 1986, ApJ, 301, 27
- Bullock J.S., Kolatt, T.S., Sigad, Y., Somerville, R.S., Kravtsov, A.V., Klypin, A.A., Primack, J.R., & Dekel, A., 2001, MNRAS, 321, 559 [astro-ph/9908159]
- Burud, I., 2002, PhD Thesis, Institut d’Astrophysique, Liege,
http://vela.astro.ulg.ac.be/themes/dataproc/deconv/theses/burud/ibthese_e.html
- Burud, I., Courbin, F., Magain, P., et al., 2002, A&A, 383, 71
- Burud, I., Hjorth, J., Jaunsen, A.O., et al., 2000, ApJ, 544, 117
- Cole S., Lacey C.G., Baugh C.M., Frenk C.S., 2000, MNRAS, 319, 168
- Courbin, F., Meylan, G., Kneib, J.P., & Lidman, C., 2002, ApJ in press [astro-ph/0202026]
- Fabbiano, G. 1989, ARA&A, 27, 87 (ASP: Provo) 25
- Falco, E.E., Gorenstein, M.V., & Shapiro, I.I., 1985, ApJ, 289, L1
- Faure, C., Courbin, F., Kneib, J.P., Alloin, D., Bolzonella, M., & Burud, I., 2002, A&A in press [astro-ph/0201057]
- Freedman, W.L., Madore, B.F., Gibson, B.K., et al., 2001, ApJ, 553, 47
- Fukugita, M., Hogan, C.J., & Peebles, P.J.E., 1998, ApJ, 503, 518
- Gerhard, O., Kronawitter, A., Saglia, R.P., & Bender, R., 2001, AJ, 121, 1936
- Gonzalez, A.H. et al., ApJ, 528, 145
- Gorenstein, M.V., Falco, E.E., & Shapiro, I.I., 1988, ApJ, 327, 693
- Guzik, J., & Seljak, U., 2002, MNRAS submitted [astro-ph/0201448]
- Hernquist, L., 1990, ApJ, 356, 359

- Impey, C.D., Falco, E.E., Kochanek, C.S., Lehar, J., McLeod, B.A., Rix, H.-W., Peng, C.Y., & Keeton, C.R., 1998, *ApJ*, 509, 551
- Jesseit, R., Naab, T., & Burkert, A., 2002, *ApJL* in press [astro-ph/0204164]
- Keeton, C.R., Christlein, D., & Zabludoff, A.I., 2000, *ApJ*, 545, 129
- Keeton, C.R., 2001, *ApJ*, 2001, 561, 46
- Kochanek, C.S., 2002a, submitted to *ApJ* [astro-ph/0204043]
- Kochanek, C.S., 2002b, submitted to *ApJ* [astro-ph/0205319]
- Kochanek, C.S., & White, M., 2001, *ApJ*, 559, 531
- Kochanek, C. S., Falco, E. E., Impey, C. D., Lehar, J., McLeod, B. A., Rix, H.-W., Keeton, C. R., Munoz, J. A., Peng, C. Y. 2000, *ApJ*, 543, 131
- Koopmans, L.V.E., de Bruyn, A.G., & Jackson, N., 1998, 295, 534
- Koopmans, L.V.E., & Fassnacht, C.D., 1999, *ApJ*, 527, 513
- Koopmans, L.V.E., de Bruyn, A.G., Xanthopoulos, E., & Fassnacht, C.D., 2000, *A&A*, 356, 391
- Lehar, J., Falco, E.E., Kochanek, C.S., McLeod, B.A., Munoz, J.A., Impey, C.D., Rix, H.-W., Keeton, C.R., & Peng, C.Y., 2000, *ApJ*, 536, 584
- Lowenstein, M., & White, R.E., 1999, *ApJ*, 518, L50
- McKay, T.A., et al., 2001, *ApJ* in press [astro-ph/0108013]
- McKay, T.A., et al., 2002, *ApJL* in press [astro-ph/0204383]
- Mo, H.J., Mao, S., & White, S.D.M., 1998, *MNRAS*, 295, 319
- Moore, B., 2001, 20th Texas Symposium, AIP#586, J.C. Wheeler & H. Martel, eds., (Melville, NY: AIP) 73
- Munoz, J.A., Kochanek, C.S., & Keeton, C.R., 2001, *ApJ*, 558, 657
- Natarajan, P., Kneib, J.-P., & Smail, I., 2001, *Gravitational Lensing: Recent Progress, Future Goals (ASP327)*, T. Brainerd, & C.S. Kochanek, eds. (ASP: San Francisco) 391
- Navarro, J.F., Frenk, C.S., & White, S.D.M., 1996, *ApJ*, 462, 563
- Netterfield, C.B., 2002, et al. [astro-ph/0104460]
- Rix, H.-W., de Zeeuw, P.T., Cretton, N., van der Marel, R.P., & Carollo, C.M., 1997, *ApJ*, 488, 702

- Romanowsky, A.J., & Kochanek, C.S., 1999, *ApJ*, 516, 18
- Saha, P., 2000, *AJ*, 120, 1654
- Schechter, P.L., et al., 1997, *ApJ*, 475, L85
- Schechter, P.L., 2000, IAU 201, A.N. Lasenby & A. Wilkinson, eds. [astro-ph/0009048]
- Schneider, P., Ehlers, J., & Falco, E.E., 1992, *Gravitational Lenses* (Berlin: Springer-Verlag)
- Seljak, U., 1994, *ApJ*, 435, 87
- Treu, T., & Koopmans, L., 2002, *ApJ* in press [astro-ph/0202342]
- Trott, C.M., & Webster, R.L., 2002, *MNRAS* submitted [astro-ph/0203196]
- Wang, X., Tegmark, M., & Zaldarriaga, M., 2002, *Phys Rev D* submitted [astro-ph/0105091]
- White, S.D.M., Navarro, J.F., Evrard, A.E., Frenk, C.S., 1993, *Nature*, 366, 429
- Witt, H.J., Mao, S., & Keeton, C.R., 2000, *ApJ*, 544, 98
- Winn, J.N., Kochanek, C.S., McLeod, B.A., Falco, E.E., Impey, C.D., Rix, H.-W., 2002, *ApJ* in press [astro-ph/0201551]